ELSEVIER

Available online at www.sciencedirect.com
SCIENCE DIRECT®

Infrared Physics & Technology 45 (2004) 181–189

INFRARED PHYSICS & TECHNOLOGY

www.elsevier.com/locate/infrared

Calculation of the R_0A product in n^+–n–p and p^+–p–n GaInAsSb infrared detectors

Tian Yuan [a,1], Soo-Jin Chua [a,b,*], Yixin Jin [c]

[a] *Department of Electrical and Computer Engineering, Center for Optoelectronics, National University of Singapore, Singapore 119260, Singapore*
[b] *Institute of Materials Research and Engineering, National University of Singapore, Singapore 119260, Singapore*
[c] *Changchun Institute of Physics, Chinese Academy of Sciences, Changchun 130021, PR China*

Received 29 April 2002

Abstract

In this paper, the zero-bias resistance areas product R_0A is calculated in the n^+–n–p and p^+–p–n $Ga_{0.8}In_{0.2}As_{0.81}Sb_{0.19}$ infrared detectors, on the base of the material parameters in the three layers. The calculated results show that parameters in the heavily doped layer in the different structures have different influences on R_0A. Moreover, R_0A in the n^+–n–p structure is higher than that in the p^+–p–n structure because the higher carrier concentration in the n^+-region for the n^+–n–p structure improves R_0A whereas the one in the p^+-region for the p^+–p–n structure reduces R_0A.
© 2003 Elsevier Ltd. All rights reserved.

Keywords: R_0A; Photodetectors; $Ga_xIn_{1-x}As_{1-y}Sb_y$; Parameters

1. Introduction

In recent years, the quaternary alloys GaInAsSb lattice matched to GaSb substrates have been increasing interest in infrared (IR) optoelectronic devices for spectral range 2–5 μm [1]. Such devices have many important applications, including gas spectroscopy analysis, remote sensing of gas pollutants, light–wave communication system using fluoride glass fibers, as well as a number of medical applications. GaInAsSb alloys have already shown their capabilities to achieve efficient lasers [2] and detectors [3–5]. One of the important figures of merit in the detectors is the zero-bias resistance areas product R_0A because the value of R_0A directly affects the detector performance expressed by the detectivity D^*. Lin et al. [6] reported the experimental results of R_0A less than 100 $\Omega\,cm^2$ in GaInAsSb detector. However, very little information can be provided from literature about the theoretical analysis of R_0A for these material detectors.

In this paper, the zero-bias resistance areas product R_0A is calculated based on the different device structures (n^+–n–p and p^+–p–n) and the

* Corresponding author. Address: Department of Electrical and Computer Engineering, Center for Optoelectronics, National University of Singapore, Singapore 119260, Singapore. Tel.: +65-68744784; fax: +65-67797454.
E-mail address: elecsj@nus.edu.sg (S.-J. Chua).
[1] Current address: Microelectronic Centre, School of Electrical and Electronic Engineering, Nanyang Technological University, 639798 Singapore.

1350-4495/$ - see front matter © 2003 Elsevier Ltd. All rights reserved.
doi:10.1016/j.infrared.2003.09.003

related material parameters. The results show: which is the optimal structure out of the two structures and what are junction depths and carrier concentrations that would maximize R_0A. The two different structures are quantitatively compared and R_0A is checked by the influence of the carrier concentrations and the junction depths in the three layers of each structure, as well as the surface recombination velocities on the two surfaces for each structure. Furthermore, on the basis of the theoretical calculation, some optimum conditions are proposed to maximize R_0A for detectors. These results are important for the fabrication of detectors.

2. Device structure and theoretical model

We consider the structures of n^+–n–p and p^+–p–n $Ga_{0.8}In_{0.2}As_{0.81}Sb_{0.19}$ detectors shown in Fig. 1, in which the lattice of $Ga_{0.8}In_{0.2}As_{0.81}Sb_{0.19}$ alloys is matched to GaSb [7]. In the p–n junction, four kinds of noise mechanism: Auger, Radiative, Generation–recombination (G–R) and tunneling, are considered and expressed by R_0A. These contributions to R_0A all add in parallel and the expressions are given in the previous paper [8]. In isotype n^+–n and p^+–p junctions, the basic assumptions are made as follows:

(1) The n^+- or p^+-region is heavily doped such that the depletion region for the n^+–n or p^+–p junction exists in the low-doped region [9]. They are shown in Fig. 1. G-R noise in the n^+–n (or p^+–p) depletion region is considered.
(2) The effective interface recombination velocities S_{pp} and S_{nn} located at the p^+–p and n^+–n junctions are introduced. They are derived to take into account the minority-carrier behavior in the heavily doped p^+- and n^+-layers [10,11].
(3) Compared to the major carrier concentration in the heavily doped layer, the minority-carrier concentration is very low; additionally the minority-carrier diffusion mechanism is determined by the interface recombination velocity. Therefore, Auger and radiative noise mechanisms in the heavily doped regions are neglected.
(4) The tunneling mechanism across n^+–n and p^+–p junctions is neglected.

The interface recombination velocities S_{pp} and S_{nn} are valid for the arbitrary p^+–p and n^+–n high-low junctions [11]:

$$S_{pp} = \frac{pD_{e_{p^+}}}{p^+L_{e_{p^+}}}\frac{r_{e_{p^+}}\cosh\left(\frac{d_{p^+}}{L_{e_{p^+}}}\right)+\sinh\left(\frac{d_{p^+}}{L_{e_{p^+}}}\right)}{r_{e_{p^+}}\sinh\left(\frac{d_{p^+}}{L_{e_{p^+}}}\right)+\cosh\left(\frac{d_{p^+}}{L_{e_{p^+}}}\right)} \quad (1)$$

$$S_{nn} = \frac{nD_{p_{n^+}}}{n^+L_{p_{n^+}}}\frac{r_{p_{n^+}}\cosh\left(\frac{t_{n^+}}{L_{p_{n^+}}}\right)+\sinh\left(\frac{t_{n^+}}{L_{p_{n^+}}}\right)}{r_{p_{n^+}}\sinh\left(\frac{t_{n^+}}{L_{p_{n^+}}}\right)+\cosh\left(\frac{t_{n^+}}{L_{p_{n^+}}}\right)} \quad (2)$$

where $D = KT\mu/q$, $L = (D\tau)^{1/2}$, $r = SL/D$.

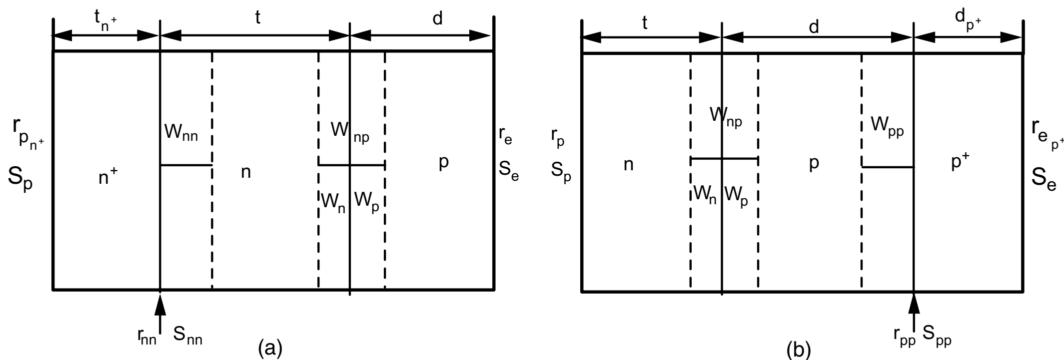

Fig. 1. The two structures for a GaInAsSb detector.

3. Calculated results and discussion

The calculations have been performed on the n^+–n–p and p^+–p–n $Ga_{0.8}In_{0.2}As_{0.19}Sb_{0.81}$ infrared detectors operated at 300 K. The basic parameters are shown in Table 1 and the related parameters have been evaluated in the same way as in the previous papers [7,8]. For practical calculation, the σ and N_f in the p–n and p^+–p (or n^+–n) junctions are assumed to be the same. Parameters except for mobilities, such as carrier concentrations, widths, surface recombination velocities, have been calculated to show how these parameters affect R_0A.

3.1. R_0A in the p^+–p–n structure

Fig. 2 shows R_0A and its components in the p^+–p–n structure as functions of p- and n-side carrier concentrations, with other parameters in Table 1

Table 1
Basic parameters for the n^+–n–p and p^+–p–n structures

Basic parameters	$T = 300$ K, $x = 0.8$, $N_f = 10^{14}$ cm^{-3}, $\sigma_s = 10^{-15}$ cm^2					
	n^+–n–p structure			p^+–p–n structure		
	n^+-region	n-region	p-region	p^+-region	p-region	n-region
Carrier concentration (cm^{-3})	5×10^{18}	10^{18}	10^{17}	10^{18}	10^{17}	10^{18}
Width (μm)	0.5	2	5	0.5	5	2
Mobility (cm^2/V s)	1000	1000	240	240	240	1000
Surface recombination velocity (m/s)	0		0	0		0

N_f and σ are respectively the trap density and capture cross-section in the depletion region.

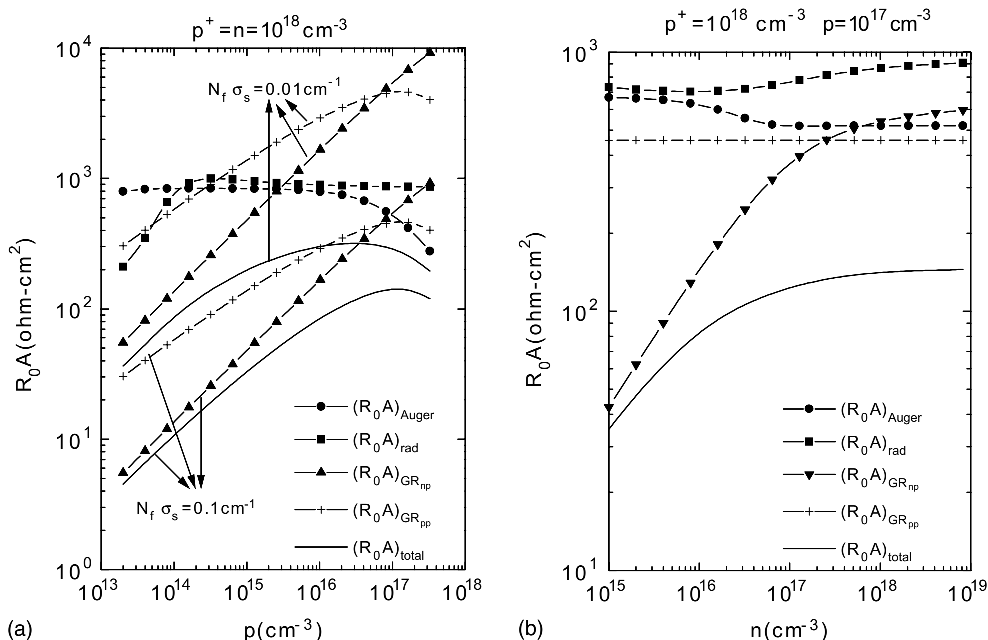

Fig. 2. The dependence of $(R_0A)_{total}$ and its components on: (a) the p-side carrier concentration (p) and (b) the n-side carrier concentration for the p^+–p–n structure.

keeping constants. Moreover, $(R_0A)_{GR_{pp}}$, $(R_0A)_{GR_{np}}$ and $(R_0A)_{total}$ with $N_f = 10^{13}$ cm^{-3} and $\sigma = 10^{-15}$ cm^2 are also plotted in Fig. 2(a). In Fig. 2(a), all of R_0A components contribute to $(R_0A)_{total}$ in $N_f = 10^{14}$ cm^{-3} and $\sigma = 10^{-15}$ cm^2, especially in $p > 10^{16}$ cm^{-3}. In the range of $p < 10^{16}$ cm^{-3}, $(R_0A)_{total}$ is mainly determined by the G-R noise in the p–n junction, while other noise components have a little contribution. Because of $(R_0A)_{GR} \propto 1/\sigma N_f$ [8], $(R_0A)_{GR}$ and $(R_0A)_{total}$ are increased if σ and N_f are reduced, which is similar to that in the n–p GaInAsSb detector [8]. In Fig. 2(a), the maximum value of $(R_0A)_{total}$ are obtained at $p = 10^{17}$ cm^{-3}. Based on this condition, Fig. 2(b) shows the dependence of $(R_0A)_{total}$ and its components on the n-side carrier concentration. $(R_0A)_{total}$ depends on all the components in $n > 10^{16}$ cm^{-3}; in $n < 10^{16}$ cm^{-3}, $(R_0A)_{total}$ is mainly limited by $(R_0A)_{GRnp}$. With increasing n, $(R_0A)_{total}$ rises up and keeps a constant in $n > 10^{18}$ cm^{-3}. No tunneling mechanism appears in Fig. 2 because the direct tunneling mechanism needs a necessary factor that both n- and p-type semiconductor materials must be degenerate. For the $Ga_{0.8}In_{0.2}As_{0.19}Sb_{0.81}$ alloy, the degeneracy state is in $p > 10^{18}$ cm^{-3} and $n > 10^{16}$ cm^{-3}.

Fig. 3 shows the dependence of $(R_0A)_{total}$ on the p-side carrier concentration with the p$^+$-side carrier concentration (p$^+$), width (d_{p^+}) and surface recombination velocity (S_e) as parameters, under the condition of other parameters in Table 1 keeping constants. $(R_0A)_{total}$ is obviously reduced with increasing p^+, d_{p^+} and S_e. The p$^+$-side parameters affect $(R_0A)_{Auger}$ and $(R_0A)_{rad}$ in the p-side through S_{pp} and $(R_0A)_{total}$. With increasing the p-side carrier concentration, the maximum value of $(R_0A)_{total}$ is obtained at $p = 10^{17}$ cm^{-3}, therefore the carrier concentration in the p$^+$-side should be higher than 10^{17} cm^{-3}. In the p–n homojunction structure, $(R_0A)_{total}$, associated with the Auger and radiative mechanisms [8], is strongly reduced by the p-side surface recombination velocity, In the triple-layer structure, it is hoped that the interface recombination velocity can be reduced with a heavily doped layer. In Fig. 3(c), although $(R_0A)_{total}$ markedly decreases in the range of $S_e > 10^4$ m/s, with the increasing of S_e from 0 to 10^2 m/s, $(R_0A)_{total}$ almost does not change. This indicates that the S_{pp} is limited by the parameters in the heavily doped layer more or less. In addition, $(R_0A)_{total}$ in Fig. 3(a) strongly decreases at $p^+ = 10^{21}$ cm^{-3} and in $p > 10^{18}$ cm^{-3} because the tunneling mechanism appears in this part.

Fig. 4 shows $(R_0A)_{total}$ with the change of the p-side width (d). $(R_0A)_{total}$ decreases with the thicker width in the p-side only in the range of $p > 10^{16}$ cm^{-3}. This result is caused by Auger and radiative noise mechanisms because only both of them are related with p-side width [12]. As shown in Fig. 2, these two noise mechanisms affect $(R_0A)_{total}$ in the range of $p > 10^{16}$ cm^{-3}. Fig. 5 shows the dependence of $(R_0A)_{total}$ on the n-side carrier concentration with the n-side width (t) and surface recombination velocity (S_p) as parameters. Although $(R_0A)_{total}$ has a little decreasing with increasing t and S_p, its optimum value is not affected by these two parameters in $n > 10^{18}$ cm^{-3}. Therefore, if the n-side carrier concentration is higher than 10^{18} cm^{-3}, the influence of these two parameters in the n-side on $(R_0A)_{total}$ can be neglected. This result is advantageous of the device fabrication because the limitation of these two parameters is canceled.

3.2. R_0A in the n$^+$–n–p structure

Fig. 6 shows $(R_0A)_{total}$ and its components in the n$^+$–n–p structure as functions of p- and n-side carrier concentrations with other parameters in Table 1 keeping constants. Moreover $(R_0A)_{GRnn}$ and $(R_0A)_{total}$ with the different n$^+$ are also plotted in Fig. 6(b). The different $(R_0A)_{GRnn}$ and $(R_0A)_{total}$ are marked as the number 1, 2 and 3. In Fig. 6(a), in the range of 10^{16} cm$^{-3} < p < 10^{18}$ cm^{-3}, $(R_0A)_{total}$ is dominated by all components and its maximum value is obtained. In $p < 10^{16}$ cm^{-3}, $(R_0A)_{GRnp}$ controls $(R_0A)_{total}$, while in $p > 10^{18}$ cm^{-3}, $(R_0A)_{tunnel}$ controls $(R_0A)_{total}$ and the tunneling mechanism strongly reduces $(R_0A)_{total}$. In Fig. 6(b), with the change of n, all of the R_0A components contribute to $(R_0A)_{total}$. The tunneling mechanism does not appear because the the p-side material is in the nondegeneracy state with p less than 10^{17} cm^{-3}. With the change of n$^+$, $(R_0A)_{Auger}$ and $(R_0A)_{rad}$ should be changed through S_{nn}, but these two mechanisms do not. With increasing n^+,

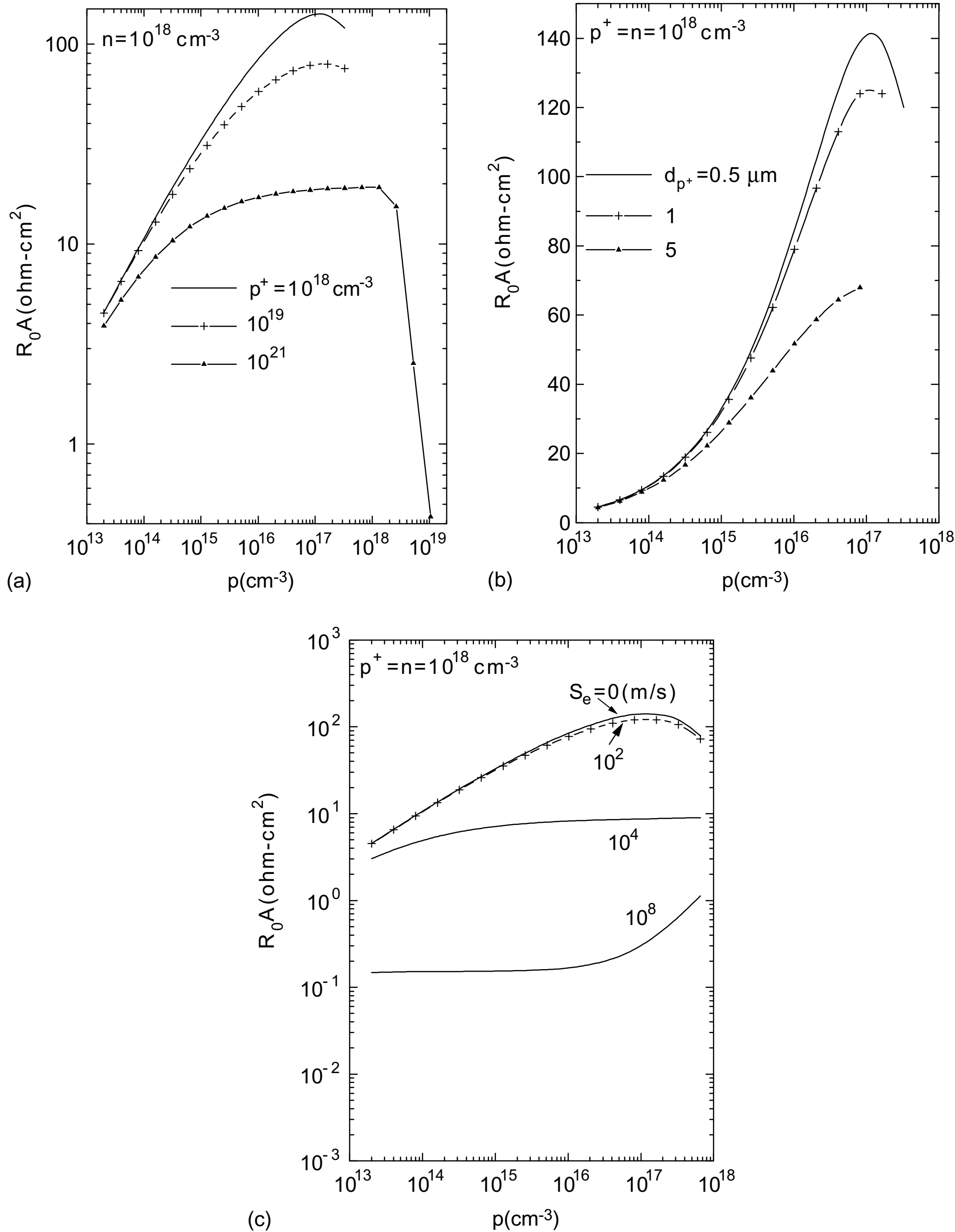

Fig. 3. The dependence of $(R_0A)_{\text{total}}$ on the p-side carrier concentration with the p^+-side: (a) carrier concentration (p^+), (b) width (d_{p^+}) and (c) surface recombination velocity (S_e) as parameters for the p^+–p–n structure.

the peak of $(R_0A)_{\text{total}}$ rises and shifts to the high n because the peak of $(R_0A)_{\text{GRnn}}$ changes in that way. That is, the high n^+-side carrier concentration is conducive to improve $(R_0A)_{\text{total}}$. With the variety of S_p and t_{n^+}, $(R_0A)_{\text{total}}$ never changes and their influence on $(R_0A)_{\text{total}}$ will be neglected. The influence of the parameters in the n^+-side for the n^+–n–p structure is completely opposite to that of the

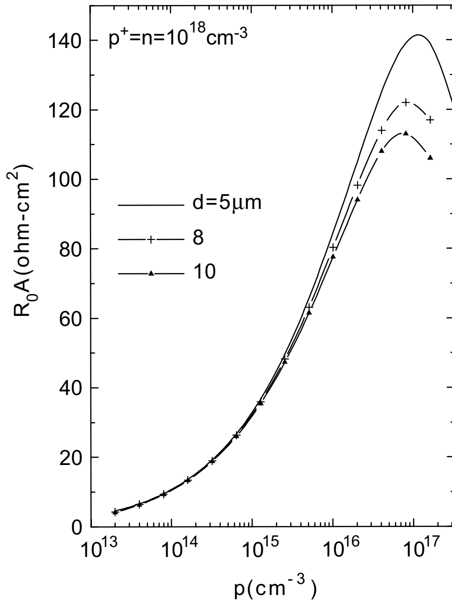

Fig. 4. The dependence of $(R_0A)_{total}$ on the p-side carrier concentration with the p-side width (d) as a parameter for the p^+–p–n structure.

parameters in the p^+-side for the p^+–p–n structure. We will discuss later. Because the influence of the n-side width on $(R_0A)_{total}$ in the n^+–n–p structure is similar to that in the p^+–p–n structure, it is neglected here.

Fig. 7 shows the influence of the p-side parameters (S_e and d) on $(R_0A)_{total}$ for the n^+–n–p structure. The parameters S_e and d are only related with Auger and radiative mechanisms. The high S_e and d reduce $(R_0A)_{Auger}$ and $(R_0A)_{rad}$ [12], therefore $(R_0A)_{total}$ decreases. Moreover, the peak of $(R_0A)_{total}$ shifts to the high p in Fig. 7(a), on the contrary to the low p in Fig. 7(b). Compare Fig. 7(a) with Fig. 3(c), except that $(R_0A)_{total}$ in the n^+–n–p structure is a little higher than that in the p^+–p–n structure at $S_e = 0$, $(R_0A)_{total}$ in the p^+–p–n structure is obviously higher than that in the n^+–n–p structure. Therefore, it is useful to add a heavily doped layer on the p-side surface for weakening the influence of the surface recombination on $(R_0A)_{total}$.

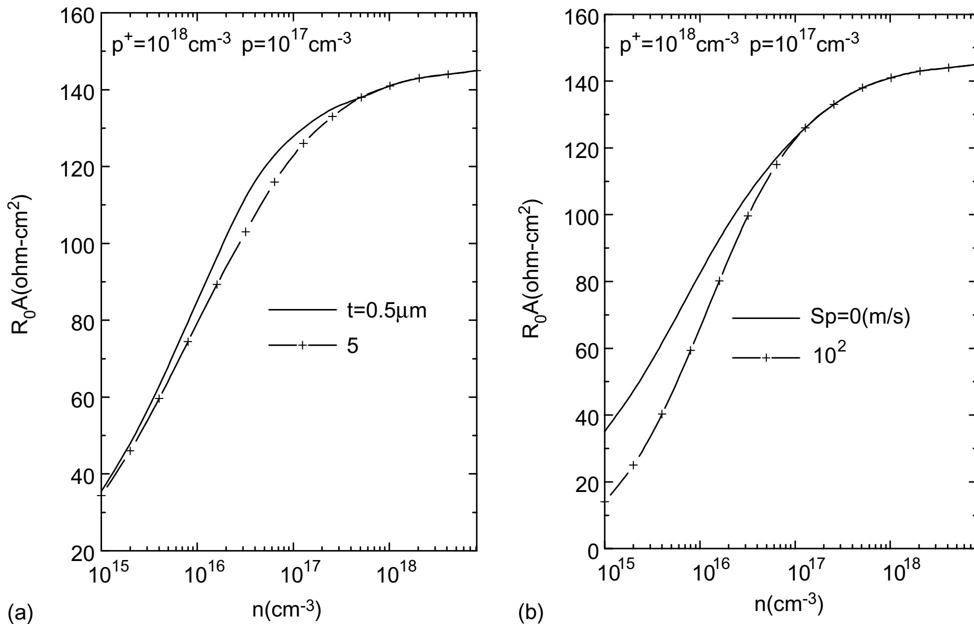

Fig. 5. The dependence of $(R_0A)_{total}$ on the n-side carrier concentration with the n-side: (a) width (t) and (b) surface recombination velocity (S_p) as parameters for the p^+–p–n structure.

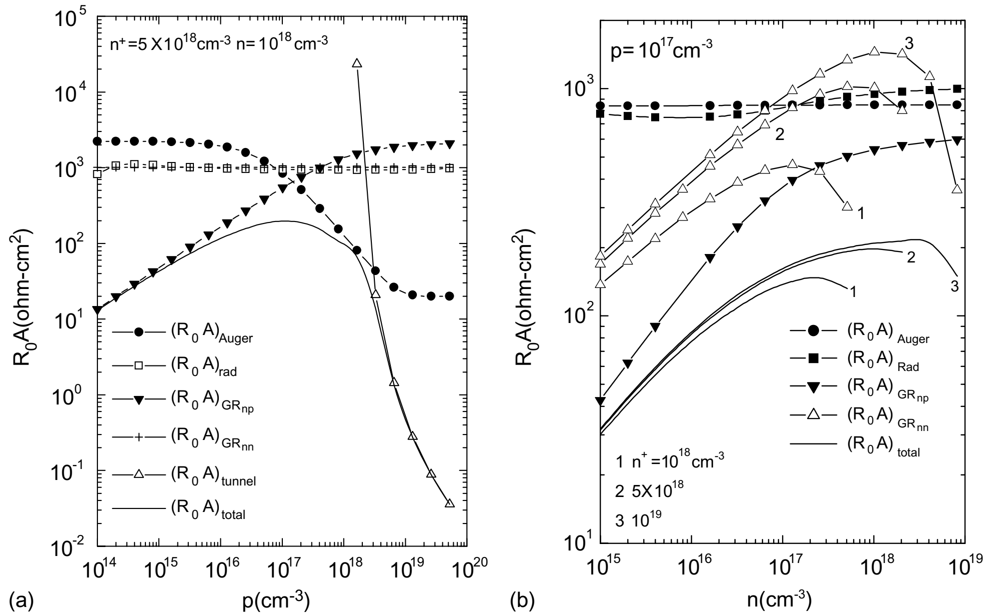

Fig. 6. The dependence of $(R_0A)_{\text{total}}$ and its components on: (a) the p-side carrier concentration (p) and (b) the n-side carrier concentration (n) for the n$^+$–n–p structure as well as $(R_0A)_{\text{GRnn}}$ with the variety of the n$^+$-side carrier concentration (n$^+$).

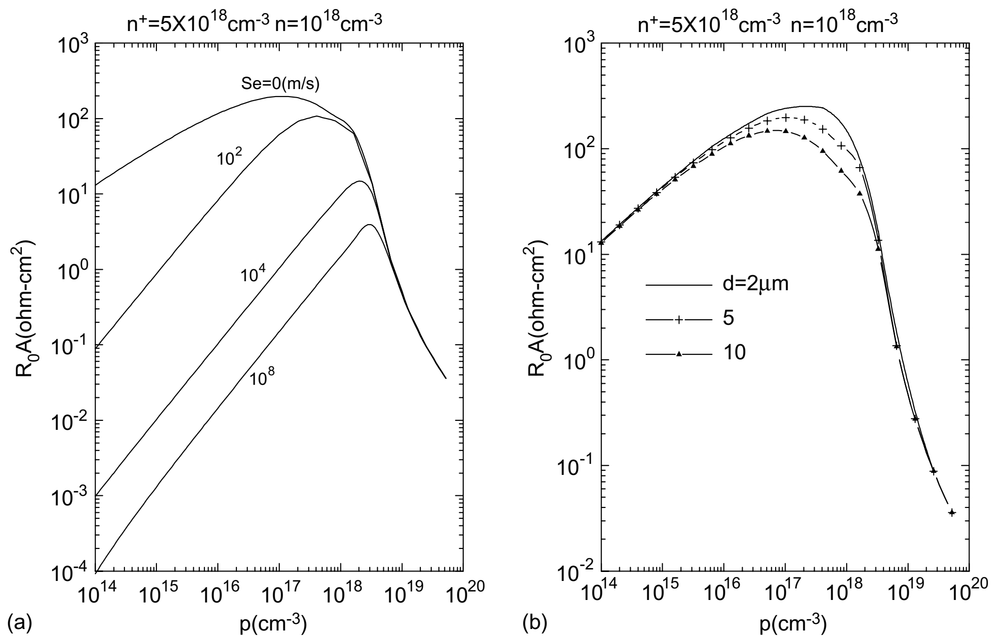

Fig. 7. The dependence of $(R_0A)_{\text{total}}$ on the p-side carrier concentration with the p-side: (a) surface recombination velocity (S_e) and (b) width (d) as parameters for the n$^+$–n–p structure.

4. Discussion

Now we discuss why the opposite results are shown in Figs. 3(a) and 6(b), and why S_p and t_{n^+} have not any influence on $(R_0A)_{total}$ in the n$^+$–n–p structure. At $n^+ = 5 \times 10^{18}$ cm^{-3}, L_{hn^+} is to be 0.0136 μm, and it will continue decreasing with the increasing of n^+, which can be considered as $L_{hn^+} \ll t_{n^+}$. Therefore S_{nn} in Eq. (2) can be approximated by $S_{nn} = \frac{nL_{hn^+}}{n^+\tau_{n^+}}$ which is not related to S_p and t_{n^+} in the n$^+$–n–p structure (τ_{n^+} is the minority-carrier lifetime in the n$^+$-side). Thus, S_p and t_{n^+} could not change $(R_0A)_{Auger}$ and $(R_0A)_{rad}$ through S_{nn} and thereby $(R_0A)_{total}$ could not be affected for the n$^+$–n–p structure. In addition, based on Ref. [8], it can be calculated that τ_{n^+} is determined by τ_{1Auger} in the n-type material [13,14], so that S_{nn} is further approximated by $S_{nn} \propto n\sqrt{1+\frac{n_i^2}{(n^+)^2}}$. In the range of $n^+ > 10^{18}$ cm^{-3}, there exists $n^+ \gg n_i$ and $S_{nn} \propto n$. This result shows that n$^+$ almost does not affect S_{nn}, and thereby not affect $(R_0A)_{Auger}$ and $(R_0A)_{rad}$ in the n$^+$–n–p structure. However with increasing the n^+-side carrier concentration, $(R_0A)_{GR}$ and $(R_0A)_{total}$ are increased in Fig. 6(b). On the contrary, in the p$^+$–p–n structure, L_{ep^+} is equal to 31.2 μm at $p^+ = 10^{18}$ cm^{-3} and to 0.032 μm at $p^+ = 10^{21}$ cm^{-3}. This shows that with increasing p^+, the variety of the relationship between L_{ep^+} and d_{p^+} is changed from $L_{ep^+} \gg d_{p^+}$ to $L_{ep^+} \ll d_{p^+}$. Therefore, in the p$^+$–p–n structure, the influence of each parameter in the p$^+$-side on $(R_0A)_{Auger}$ and $(R_0A)_{rad}$ associated with S_{pp} could not be neglected, and correspondingly, $(R_0A)_{total}$ is changed by the variety of the parameters in the p$^+$-side.

Fig. 8 shows the variety of S_{pp} and S_{nn} with S_e and S_p respectively. As above discussions, S_{nn} is not affected by S_p, which shows a horizontal line in Fig. 8. However S_{pp} increases in $10 < S_e < 10^7$ m/s. The two limiting values of the surface recombination velocity are $S = 0$ and $S = \infty$. The former implies an ideal ohmic contact whereas the latter means an ideal majority-carrier contact. In practice, the contact at the p$^+$-region surface of a p$^+$–p–n structure is a nonideal majority-carrier contact and is found to have a value of S_e that is finite and greater than zero. In Fig. 8, although S_{pp} has a high value (>10 m/s) in $S_e < 10$ m/s, S_{pp} is obviously lower than S_e in $S_e > 10$ m/s. This result demonstrates that adding a layer will effectively reduce the influence of the surface recombination on GaInAsSb photodetectors. In Ref. [6], the authors have mentioned that the surface leakage current is an important factor to influence R_0A, which increases as the surface recombination is suppressed. Basing on our simulation results, we provide a suitable structure to limit the surface recombination. In addition, utilizing the high-low junction can minimize minority-carrier recombination losses [15]. Therefore the detectors properties are improved for triple-layer structures.

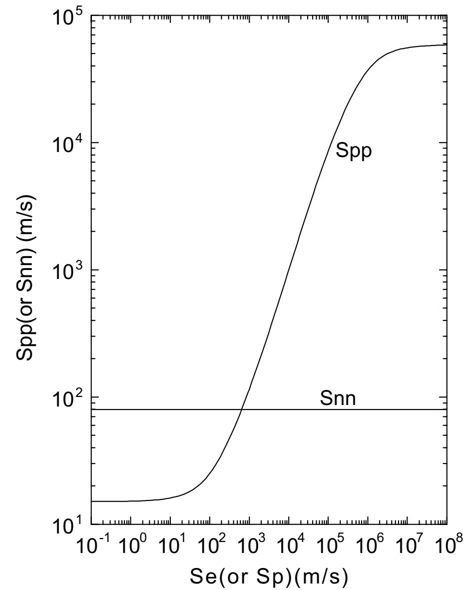

Fig. 8. The dependence of the interface recombination velocities S_{pp} and S_{nn} on the S_e and S_p for the p$^+$–p–n and n$^+$–n–p structures respectively.

5. Conclusion

In this paper, four kinds of noise mechanisms are considered for R_0A in the n$^+$–n–p and p$^+$–p–n $Ga_{0.8}In_{0.2}As_{0.81}Sb_{0.19}$ infrared photodetectors. $(R_0A)_{total}$ with these noise mechanisms are calculated based on the material parameters in the three

layers. The main conclusions can be drawn from the above study as follows:

(1) In the p^+–p–n structure, the parameters in the p^+-side affect $(R_0A)_{\text{Auger}}$ and $(R_0A)_{\text{rad}}$ through S_{pp} and hence $(R_0A)_{\text{total}}$. The high $(R_0A)_{\text{total}}$ is obtained with the low carrier concentration and the surface recombination velocity as well as the thin width in the p^+-side. In addition, the thick width in the p-side reduces $(R_0A)_{\text{total}}$. However, although $(R_0A)_{\text{total}}$ has a little decreasing with the thick width and the high surface recombination velocity in the n-side, the optimum value of $(R_0A)_{\text{total}}$ could not be affected by these two parameters in the n-side carrier concentration higher than 10^{18} cm^{-3}.
(2) In the n^+–n–p structure, the n^+-side carrier concentration is required to be as high as possible in order to obtain the high $(R_0A)_{\text{total}}$ and at the same time, the carrier concentration in the n-side should be increased, while the width and the surface recombination in the n^+-side and n-side almost do not influence $(R_0A)_{\text{total}}$. In addition, the low surface recombination velocity and the thin width in the p-side is required to obtain the high $(R_0A)_{\text{total}}$.
(3) Compared the influence of the surface recombination velocity in the p^+-side in the p^+–p–n structure with that in the p-side in the n^+–n–p structure on $(R_0A)_{\text{total}}$, it is found that, except that $(R_0A)_{\text{total}}$ in the n^+–n–p structure is a little higher than that in the p^+–p–n structure at $S_e = 0$, $(R_0A)_{\text{total}}$ in the p^+–p–n structure is obviously higher than that in the n^+–n–p structure. This result indicates that it is useful to add a heavily doped layer on the p-side surface for weakening the influence of the surface recombination on $(R_0A)_{\text{total}}$.

References

[1] B. Zhang, Y. Jin, T. Zhou, H. Jiang, Y. Ning, S. Li, Mar. Res. Soc. Symp. Proc. 415 (1996) 31.
[2] H.K. Choi, S.J. Eglash, Appl. Phys. Lett. 59 (1991) 1165.
[3] A. Aardvark, G.G. Allogho, G. Bougnot, J.P.R. David, A. Giani, S.K. Haywood, G. Hill, P.C. Klipstein, F. Mansoor, N.J. Mason, R.J. Nicholas, F. Pascal-Delannoy, M. Pate, L. Ponnampalam, P.J. Walker, Semicond. Sci. Techno. 1S (1993) S380.
[4] A.K. Srivastave, J.C. Dewinter, C. Caneau, M.A. Pollack, J.L. Zysdind, Appl. Phys. Lett. 48 (1986) 903.
[5] B. Zhang, T. Zhou, H. Jiang, Y. Ning, Y. Jin, Electron. Lett. 31 (1995) 830.
[6] C. Lin, Y.L. Zheng, A.Z. Li, J. Cryst. Growth 227–228 (2001) 605.
[7] Y. Tian, T. Zhou, B. Zhang, Y. Jin, Y. Ning, H. Jiang, G. Yuang, Opt. Eng. 37 (1998) 1754.
[8] Y. Tian, T. Zhou, B. Zhang, Y. Jin, H. Jiang, J. Phys. D 31 (1998) 3291.
[9] S. Singh, P. Singh, IEEE Trans. Electron. Dev. 38 (1991) 337.
[10] J. Hauser, P. Dunbar, Solid-State Electron. 18 (1975) 15.
[11] J. Alamo, J. Meerbergen, F. D'Hoor, J. Nijs, Solid-State Electron. 24 (1981) 533.
[12] Y. Tian, T. Zhou, B. Zhang, H. Jiang, Y. Jin, IEEE Trans. Electron. Dev. 46 (1999) 656.
[13] M. Takeshima, J. Appl. Phys. 43 (1972) 4114.
[14] A. Beattie, G. Smith, Phys. Status Solidi 19 (1967) 577.
[15] A. Lugue, A. Cuevas, J. Eguren, Solid-State Electron. 21 (1978) 793.